Charge measurement and control for the Gravity Probe B gyroscopes

Saps Buchman, Theodore Quinn, G. M. Keiser, and Dale Gill
W. W. Hansen Experimental Physics Laboratory, Stanford University, Stanford, California 94305

T. J. Sumner
Astrophysics Group, Imperial College, London, United Kingdom

(Received 31 August 1993; accepted for publication 27 September 1994)

We describe a technique based on photoemission for controlling the charge of the Gravity Probe B electrostatically suspended gyroscopes, and three methods for measuring this charge. Charging is caused by cosmic radiation in orbit and by enhanced field emission in ground testing. Errors induced by disturbing torques require the potential of the gyroscope to be smaller than 15 mV (15 pC) during the space experiment. The disturbing drift rate produced by measuring and controlling the charge in orbit is smaller than 10^{-13} deg/h, as compared with the 10^{-11} deg/h systematic drift rate of the gyroscope. The charge control technique is based on ultraviolet photoemission of electrons from both the gyroscope and a charge control electrode on the gyroscope housing. We demonstrate the effectiveness of this method in ground testing and therefore its suitability for the space experiment. Calculations indicate that heating by absorbed photons is, in the worst case, smaller than 1 nW and thus not a problem for the experiment. The principal charge measurement method is based on the determination of the control effort needed to balance a force modulation applied to the suspension electrodes. This technique is insensitive to pickup from the suspension system and to gyroscope miscentering, and is independent of the gyroscope acceleration. We demonstrate that the force modulation method is suitable for charge monitoring in orbit with an accuracy equal to or better than 4 mV.

I. INTRODUCTION

This paper presents the techniques developed to measure and control the charging of the Gravity Probe B[1] (GP-B) gyroscopes. Charging significantly degrades gyroscope performance and, if not controlled, can jeopardize the experiment. While specifically developed for GP-B, these techniques are generally applicable for noncontact bipolar charge measurement and control of levitated systems.

GP-B, also known as the Stanford Relativity Mission, is designed to provide a fundamental test of the theory of General Relativity by measuring the geodetic and frame-dragging effects of the Earth on the precession of very precise gyroscopes in a 650 km altitude polar orbit. Schiff[2] has calculated the relativistic precession $\mathbf{\Omega}$ for a gyroscope in a circular Earth orbit to be

$$\mathbf{\Omega}=\frac{3GM}{2c^2R^3}(\mathbf{R}\times\mathbf{v})+\frac{GI}{c^2R^3}\left[\frac{3\mathbf{R}}{R^2}(\boldsymbol{\omega}_e\cdot\mathbf{R})-\boldsymbol{\omega}_e\right], \tag{1}$$

where $\mathbf{R}$ and $\mathbf{v}$ are the location and the orbital velocity of the gyroscope, and I, M, and $\vec{\omega}_e$ are the moment of inertia, the mass, and the angular velocity of the Earth.

The first term represents the geodetic effect. It causes a 6.6 arcsec/yr precession rate for the 650 km polar orbit of the GP-B gyroscopes, and it is due to the motion of the gyroscope through the curved space time around the Earth. The geodetic effect will be measured to about two parts in 10^5, thus providing the most precise test to date of any of the positive predictions of general relativity. The second term represents the effect due to the dragging of the inertial frame by the rotation of the Earth. It results in a precession rate of 0.033 arcsec/yr, to be measured with a precision of about 1%. This will represent the first measurement of the frame dragging effect. The two precessions are measured by referring the local frame, determined by the gyroscopes, to the universal inertial frame, determined by a telescope pointed to a remote star, namely HR5110. Note that the proper motion of the star must be determined in a separate experiment. The experiment will be placed in a drag-free satellite.[3] As shown schematically in Fig. 1, the polar orbit will result in orthogonal geodetic and frame-dragging precessions, thus significantly simplifying the data analysis.

Figure 2 is a schematic exploded view of the gyroscope and its housing. The gyroscope consists of a 1.9 cm radius fused quartz sphere coated with a 1.3 μm film of niobium, enclosed and suspended in a fused quartz housing.[4] Three orthogonal pairs of sputtered thin film electrodes are coated on the housing cavity. The spacing from the electrodes to the centered gyroscope is 32 μm and the suspension is based on applied electrostatic forces. The area between the electrodes of the gyroscope housing cavity is coated with a 2000 Å film of titanium in order to avoid buildup of electric charges on the fused quartz. This film also serves as an additional dc support electrode in the ground testing of the gyroscope. It increases the total electrostatic support area, thus decreasing the required support field. The gyroscopes will have a drift rate of less than 0.3 marcsec/yr (10^{-11} deg/h). Figure 3 represents schematically the four gyroscopes, the drag-free sensor, and the telescope assembled in a quartz block which is used for alignment and mechanical stability. This instrument assembly is inserted in a vacuum probe which in turn is enclosed in a 1500 ℓ superfluid liquid helium flight dewar.

The readout system is based on the spinning superconducting shell of the gyroscope producing a magnetic dipole moment, also known as the London moment,[5] which is aligned with the instantaneous spin axis (and consequently,

 0034-6748/95/66(1)/120/10/$6.00

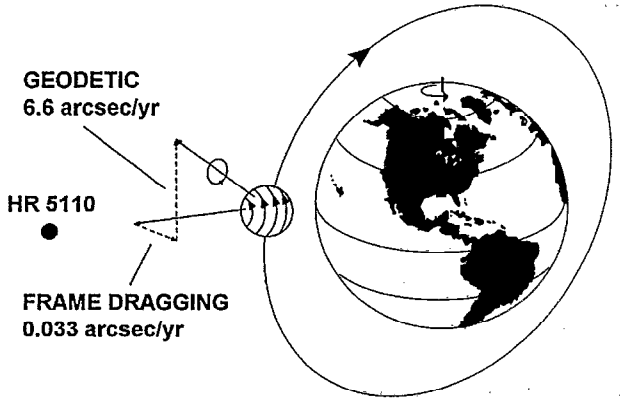

FIG. 1. GP-B geodetic and frame-dragging precessions predicted by General Relativity.

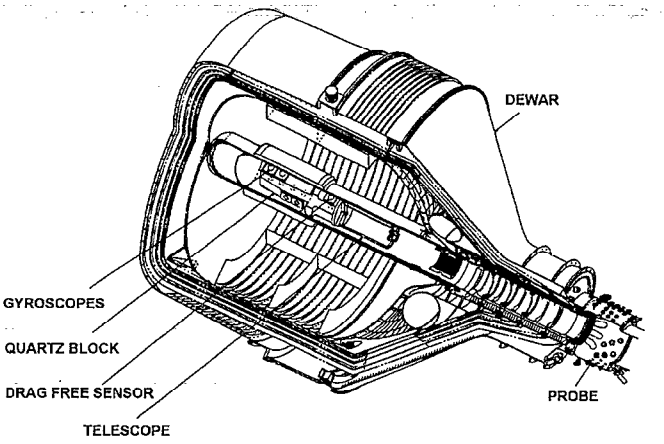

FIG. 3. Schematic view of the GP-B instrument with vacuum probe and dewar.

for a very good sphere, with the angular momentum vector). Changes in the orientation of the angular momentum cause variations in the magnetic flux through a pickup loop, which are measured by a superconducting quantum interference device (SQUID) coupled magnetometer.

The GP-B gyroscopes are required to operate in two distinct regimes; in full Earth gravity ($1g$) for the purpose of development and testing, and in the ultralow acceleration environment ($<10^{-7}$ g) achieved during the 18-months science mission flight. An additional requirement limits the fluctuations of the temperature difference between the gyroscopes and the 2 K gyroscope housings to less than 2 K. This last requirement ensures the dimensional stability of the gyroscope and limits the amount of helium desorption from its surface.

Gyroscope levitation on the ground, in the 1 g environment, requires voltages of about 1000 V peak value for the electrostatic suspension. This corresponds to electric fields of the order of 3×10^7 V/m between the gyroscope and the suspension electrodes, a value at which electron field emission becomes significant.[6] The field emission current can be as large as 1 nA, resulting in a worst-case charging rate of 1 V/s (1000 pF total gyroscope capacitance), and a maximum gyroscope potential of about 500 V. In good quality gyroscopes these values are $\leq$1 pA and $\leq$30 V, respectively. For the niobium-coated gyroscope and the titanium-coated electrodes the emission current is predominantly in the gyroscope direction, resulting in a negative charge accumulation. Charge control in this regime would therefore typically require removal of the negative charge from the gyroscope.

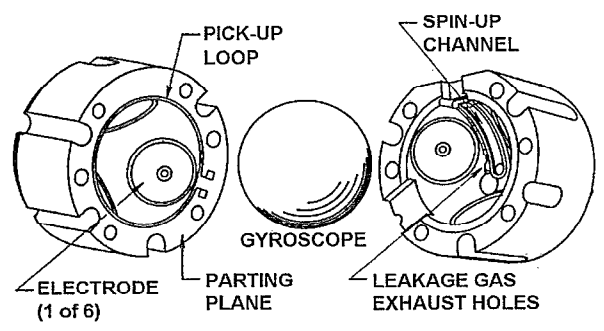

FIG. 2. Exploded view of the GP-B quartz gyroscope assembly.

The increased electric field stress due to the addition of the gyroscope potential to the suspension voltage can result in electric breakdown and possible de-levitation. In addition, we observe a strong correlation of the gyroscope charging with an anomalous, spin-speed independent, spin-down rate. We attribute this spin down to a hysteretic loss mechanism dependent upon gyroscope charging. The goal for ground testing charge control is zero gyroscope charge for the case with no supplementary dc support, or zero gyroscope voltage for the case with dc support.

The peak acceleration level on the gyroscope in the space mission drag-free satellite is of the order of 10^{-7} g (due to the gradient in the Earth's gravitational field), resulting in suspension voltages of about 0.3 V peak value, and electric fields of 10^4 V/m. No field emission takes place in these conditions. The electrostatic suspension system allows for five overlapping suspension levels between 1 and 10^{-7} g. Gyroscope charging in space is caused by three mechanisms: cosmic radiation, gyroscope levitation, and gyroscope spin up. Cosmic radiation charging is caused mainly by high energy protons stopping in the gyroscope. The primary electron flux is eliminated by the approximately 20 g/cm^2 aluminum equivalent shielding, while the production rate of secondary electrons is significantly smaller than unity. Cosmic radiation causes the gyroscope to charge positively with a rate of about 6×10^9 protons/yr ($\sim$1 V/yr). This value is above the 0.3 V suspension voltage, and well above the 15 mV maximum gyroscope potential allowed for in the experimental error budget for the Newtonian torques.

The amplitude and sign of the charging due to gyroscope levitation and spin up are difficult to estimate. However, this charging occurs only at the beginning of the experiment, when the helium gas pressure is above 10^{-6} mbar and therefore the gas conductivity is significant. Under these conditions charge control UV power of up to 1 μW are allowable, as compared to 1 nW during the high vacuum (10^{-11} mbar) main experimental period. Charge control in space requires therefore neutralization of the positive charging during the

main sequence of the mission, and neutralization of a charge of unknown sign and with amplitude of up to 6×10^{10} protons ($\sim$10 V) at the beginning of the mission (following the initialization operations of levitation and spin up).

The charge control technique we developed for GP-B is based on ultraviolet photoemission of electrons from both the gyroscope and a charge control electrode on the wall of the gyroscope housing. It has the capability of both adding and removing electrons to and from the gyroscope, thus controlling both positive and negative gyroscope charging. In this paper we demonstrate the effectiveness of this technique. Calculations indicate that gyroscope heating by absorbed photons should be, at worst, comparable to the heating caused by cosmic radiation which constitutes the main steady-state charging mechanism. Thus the temperature of the gyroscope will remain in the allowable range of 2–4 K.

We use three methods for the measurement of the gyroscope charge.

The principal charge measurement method is based on measuring the gyroscope motion induced by a force modulation applied to the electrodes. The modulation frequency is about 1% of the suspension system bandwidth, with equal amplitudes and 180° phase difference for opposite electrodes. This method is insensitive to pickup from the suspension system and independent of the gyroscope acceleration. Measurements indicate that the force modulation method is suitable for charge monitoring in orbit, achieving a gyroscope potential measurement accuracy of 4 mV (4pC). This method is being implemented in the baseline suspension system design for GP-B, and will be used for charge measurement both in space and on the ground.

The second method, referred to as the $\omega/2\omega$ technique, is based on measuring the components of the gyroscope motion at the suspension system frequency and at twice this frequency (along each of the three suspension axes). For a centered gyroscope the charge is then proportional to the ratio of these two measurements, and is determined redundantly by a three-axis measurement. This method does not require any additions to the suspension electronics. Its main disadvantages are (a) linear dependence on the gravitational acceleration, which makes it unusable in orbit, and (b) sensitivity to pickup from the suspension system signal. The accuracy of this method is about 30 V (30 nC) in Earth gravity conditions, making it well suited for ground testing.

The third charge measurement method makes use of the supplementary dc suspension electrode used in specialized ground tests. We determine the gyroscope charge by measuring the dc support voltage needed to reduce the ac support effort to zero. This technique has an accuracy of about 5 V (5 nC), and is used for ground testing with supplementary dc support. It is not usable in space.

II. GYROSCOPE CHARGING MECHANISMS

The principal gyroscope charging mechanism during ground testing is the enhanced field emission caused by the large electric fields (3×10^7 V/m) required for levitation. The asymmetry in the enhanced field emission between the niobium coating of the gyroscope and the titanium coating of the electrodes results in a predominantly negative charging

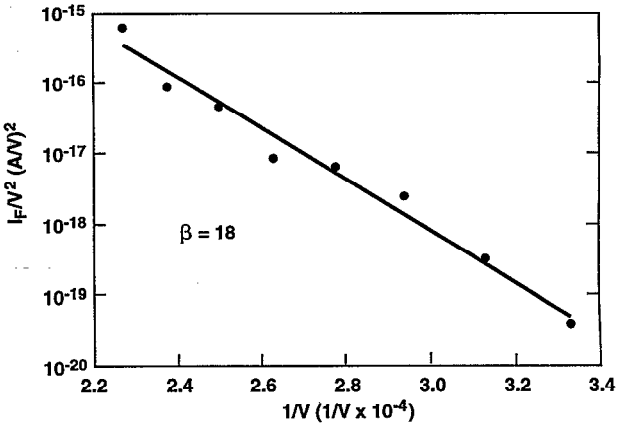

FIG. 4. Fowler–Nordheim (Ref. 6) plot for a suspension electrode trilayer coating: Ti(100 nm)-Cu(2500 nm)-Ti(250 nm). The field enhancement factor β equals 18.

of the gyroscope. Testing has confirmed that the current flow in the gyroscope follows the field dependence given by the Fowler–Nordheim formula[6] for the field emission current I_F (A)

$$I_F = C_1 A_e (E\beta)^2 e^{-C_2/(E\beta)}, \tag{2}$$

$$C_1 \equiv (1.54\times10^{-6})\frac{1}{\phi}\, e^{10.41/\sqrt{\phi}}, \tag{2a}$$

$$C_2 \equiv (6.53\times10^{9})\phi^{1.5}, \tag{2b}$$

where A_e (m^2) is the emitting area, E (V/m) is the applied electric field, β is the enhancement factor due to surface irregularities, and ϕ (eV) is the work function for the metal (typically $\phi\approx4$ eV).

Figure 4 shows the Fowler–Nordheim plot measured with a gap of 25 μm for the standard electrode trilayer film of Ti(100 nm)-Cu(2500 nm)-Ti(250 nm). The field enhancement factor β for the electrodes is typically around 20, while the niobium gyroscope coating has a β factor 10%-20% lower. Figure 5 shows the applied electric field (at 25 μm) which produces a 2 pA field emission current for various films tested for the gyroscope and the suspension electrodes. Notice the difference between the gyroscope coating and the best electrode coating Ti-Cu-Ti. The exact field emission current depends also on the preparation of the surfaces and on their conditioning under high electric fields. Coatings consisting of seven-layer sandwiches of titanium and copper further reduce the enhanced field emission.[7] The GP-B flight gyroscopes do not exhibit measurable charging (less than 10 V potential) during ground testing for both room temperature and liquid helium temperature operation.

Cosmic radiation is expected to disturb a number of experimental subsystems: the electronics, the readout system, and the gyroscopes themselves. The electronic system will be made immune to single event upsets and latch ups. Possible cosmic radiation induced readout effects include trapped flux movement and generation in the SQUIDs and the superconducting pickup loops. GP-B studies show that these effects are too small to influence the accuracy of the

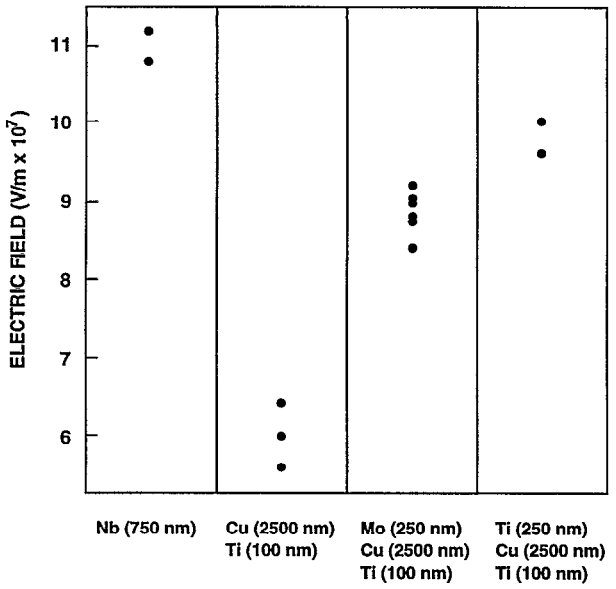

FIG. 5. The electric field required for an electron field emission current of 2pA for different electrode and gyroscope coatings. The measurements indicate the repeatability of the experiment.

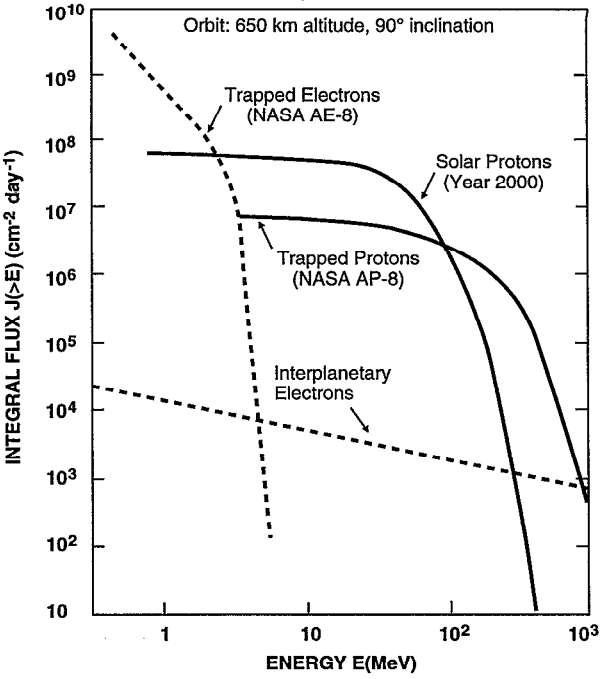

FIG. 6. Cosmic radiation background for the GP-B satellite (Refs. 8 and 9). The solar proton flux is the yearly averaged median for the year 2000.

experiment. The radiation effects on the gyroscope are: heating, charging, torquing by momentum transfer, and induced flux motion in the gyroscope coating. The torques produced by cosmic radiation are negligible, while gyroscope heating and trapped flux motion are manageable and are the subjects of ongoing investigations. This paper concentrates on the solution of the problem of gyroscope charging by cosmic radiation only.

Cosmic radiation is the principal continuous source of gyroscope charging during the GP-B science mission. Figure 6 shows the daily flux rates of protons and electrons for the GP-B orbit at 650 km altitude and 90° inclination. The trapped particle flux is given by the NASA/NSSDC models[8] AP-8 for protons and AE-8 for electrons, while the solar proton flux[9] is the mean expected level for the year 2000, the projected GP-B flight date.

The gyroscope shielding is about 20 g/cm^2 aluminum equivalent, allowing only electrons with energies in excess of about 55 MeV to reach the gyroscopes. There are no trapped electrons at these energies, and consequently the problem of charging by trapped electrons is eliminated. Interplanetary electrons will contribute to the negative charging of the gyroscopes. However, their flux at around 55 MeV is more than two orders of magnitude smaller than the proton flux at energies which penetrate the shielding, making this contribution to charging negligible. We conclude therefore that the primary contributors to gyroscope charging are the trapped and solar flare protons, and we proceed to calculate the charging rate.

Inverting the Bethe–Bloch formula[10] for energy loss dT/dx per distance traveled in a material, we obtain the penetration range R

$$R=\int \frac{dT}{(dT/dx)} = \int_{T_0}^{T_f} \frac{4\pi\epsilon_0 m v^2}{ne^4} \frac{1}{\ln\left(\frac{2\gamma^2 m v^2}{I}\right)-\frac{v^2}{c^2}}\, dT, \tag{3}$$

where T, m, v, e, and γ are the kinetic energy, mass, velocity, charge, and relativistic γ factor of the proton, and $n \equiv N_A Z/A$ and I are the electron density and the average ionization potential of the material.

We are interested in the energy range of protons that come to a stop inside the gyroscope after passing through the materials of the science mission probe assembly. This range is 140–205 MeV. Using the proton fluxes of Fig. 6, we obtain a total flux of stopped protons of about 6×10^9 protons/yr, where about half of the flux is contributed by the solar protons. This translates into a positive potential increase rate of 1 V/yr, which would exceed in one week the limit of 15 mV for the operation of the GP-B gyroscopes.

We consider next the mechanism of negative charging of the gyroscope by secondary electron emission. Protons will ionize atoms in their path and generate electrons with an energy smaller than 1 keV, corresponding to a maximum range in quartz of about 10 μm. The flux of secondary electrons Φ_e is given by

$$\Phi_e = \int \frac{d\Phi_p(T)}{dT} Y(T) dT, \tag{4}$$

where $\Phi_p(T)$ and $Y(T)$ are the energy-dependent proton flux at the gyroscope surface and the energy-dependent production rate of secondary electrons.[11] The integration results in a yield of 0.025 electrons per proton for the energy distribution

of the trapped protons, and a yield of 0.050 electrons per proton for the solar flare protons. Charging by secondary electrons can be thus neglected, leaving the gyroscope charging at plus 1 V/yr. This result has been checked by interpolating the charging data for the drag-free sensor of the CASTOR/CACTUS experiment[12] (230 km perigee, 1250 km apogee, 30° inclination) to the GP-B orbit. For both missions the main trapped proton flux is due to the South Atlantic Anomaly,[13] the region of minimum magnetic field and consequently of maximum trapped proton density.

Two additional charging mechanisms are caused by gyroscope levitation (separation of dissimilar metals) and by the spin up of the gyroscope with helium (partially ionized gas). The magnitude and the sign of the charging due to these mechanisms is difficult to predict; however, experiments place an upper bound of ±30 V on the gyroscope charging they produce. Both of these effects take place in the initialization stage of the experiment, during which the thermal constraints on the gyroscopes are much less severe than during the actual experiment.

III. ULTRAVIOLET PHOTOEMISSION CHARGE CONTROL TECHNIQUE

We have considered several nonintrusive charge sources for GP-B charge control, including radioactive sources, ion sources, and Spindt-type field emission cathodes,[14] but have selected UV photoemission as our charge source for the following reasons:

(a) Both positive and negative charge flow is easily obtainable through appropriate biasing of a charge control electrode.
(b) The UV source is easily controlled.
(c) The UV flux can be "piped in" via fiber optics from a remote UV source to the restricted access region near the gyroscope.

Figure 7 shows a schematic of the basic UV photoemission charge control concept. Both the surface of the gyroscope and the surface of a charge control electrode are illuminated with UV light, inducing photoemission from both surfaces. The direction of the resulting charge flow is controlled by appropriate biasing of the charge control electrode with respect to the gyroscope surface. Experimental considerations dictate that the gyroscope surface be a sputtered thin film of niobium, but we are free to choose the material of the charge control electrode subject to the standard constraints on hardware near the gyroscope: nonmagnetic, very clean, and nonsuperconducting at the experiment temperature of 2 K.

Due to UV power limitations imposed by fiber optic coupling, the primary consideration for selecting a charge control electrode material is clearly its quantum efficiency (the average number of photoelectrons emitted by a surface per incident photon). Figure 8 shows the quantum efficiency as a function of photon wavelength for various pure metal surfaces prepared in vacuum.[15] It indicates large differences in quantum efficiency between various metals, with Be and Mg apparently being the most promising candidates as charge control electrode materials. At the 253.7 nm line of Hg arc lamps, for example, Be and Mg have quantum efficiencies in the 10^{-1}–10^{-2} range while niobium (which is taken to be the same as V, Ti, and Cr) should be in the 10^{-5}–10^{-6} range.

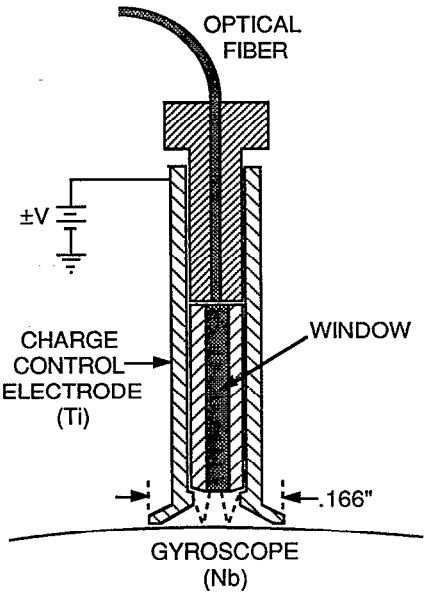

FIG. 7. Schematic representation of the UV charge control arrangement for the GP-B gyroscopes.

In practice, though, it is impossible to prepare and maintain the metal surfaces near our gyroscope in vacuum, so we might expect large deviations from this data due to oxide layers and other contaminants on the surfaces. We have measured the quantum efficiencies of various samples prepared in conditions which reflect the preparation and cleaning procedures for the gyroscopes. The apparatus was at room tem-

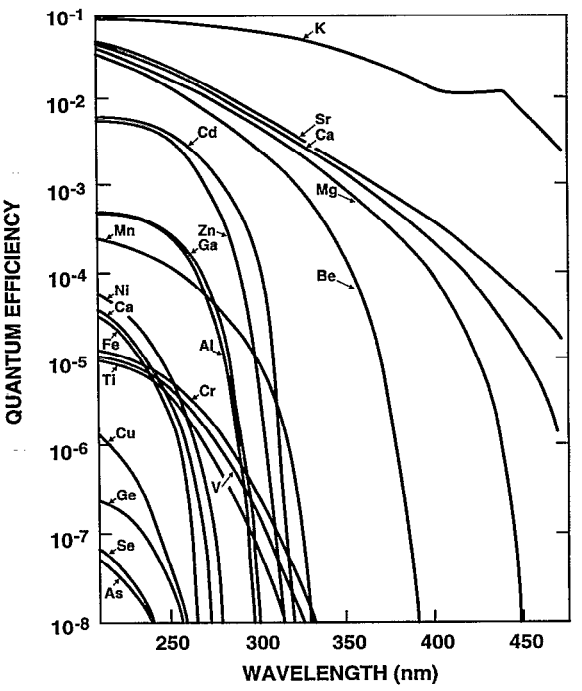

FIG. 8. Photoelectric quantum efficiency for some metals as a function of wavelength (Ref. 15).

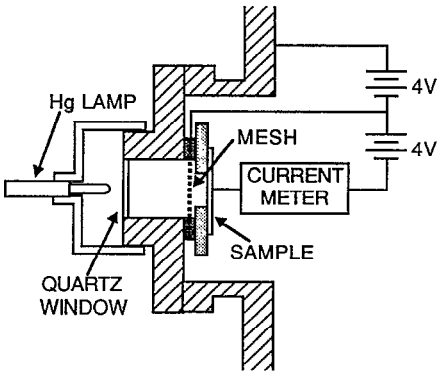

FIG. 9. Schematic of experimental setup for the UV photoemission efficiency measurement.

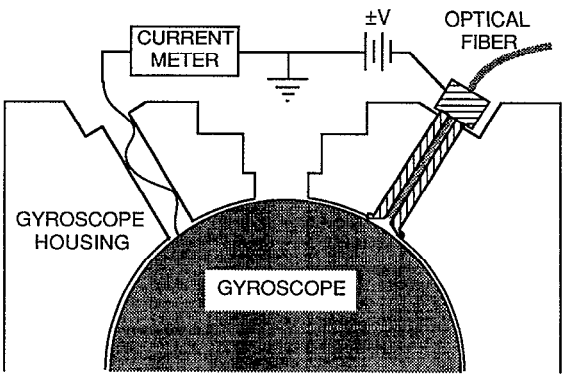

FIG. 10. Schematic of experimental setup for the measurement of UV generated currents in the gyroscope.

perature and the pressure in the region of the sample was on the order of 10^{-7} Torr. Figure 9 is a schematic representation of this apparatus.

As expected, the collection of photoemitted electrons saturated at a sample bias of 3–4 V, so all of the photoemission measurements were taken with a 4 V bias between the sample and the mesh with the sample being most negative. Also, the mesh and the sample were floated 4 V negative with respect to the surrounding vacuum can. The photoemission current was taken to be the current measured between the sample and the mesh. Measurement of the output of the ac Hg discharge lamp[16] with an UV photometer at 1.3 cm distance gave a value of 0.55 mW/cm^2 in the 400 nm region for which the photometer was calibrated. From the lamp spectrum included in the manufacturer's literature, we expect this output to be 12% of the total output in the 253.7 nm line of interest. Correcting for this factor as well as the sample's distance and area, we calculated the total UV power delivered to the sample in the 253.7 nm line of 3.1×10^{-3} W. Since we do not know how many reflections were taking place for an average photon in this system, we associate this total power with a minimum photon flux and hence calculate an upper bound for the quantum efficiency of each of the materials. Table I gives a summary of these measurements.

Two aspects are interesting about these data. First, the quantum efficiency of all of the "apparatus-grade" materials is clearly much lower than the quantum efficiency of comparable pure materials prepared in vacuum as described by Fig. 8. Second, there does not seem to be a significant difference (more than an order of magnitude) between the quantum efficiencies of the various materials under these conditions of cleanliness and environment. In light of these data, we tentatively selected Ti as our charge control electrode material since its properties are compatible with the requirements of the gyroscope environment.

Figure 10 shows the setup we used to test a prototype of the photoemission charge control equipment. The apparatus was at room temperature and the pressure in the region of the gyroscope and the charge control electrode was of the order of 10^{-7} Torr. Direct electrical connection was made to the surface of an unlevitated gyroscope with a 0.13 mm copper wire pressed against its surface through one of the housing access holes. The gyroscope's surface was connected to ground through a current meter and the photoemission current was taken to be the current between ground and the gyroscope's surface. We illuminated both the gyroscope surface and, by reflection, the surface of the charge control electrode with light from a 300 μm core UV-transparent optical fiber. As before, photoemission in each direction tended to saturate at just a few volts of bias, so a bias of 3 V was used between the gyroscope surface and the charge control electrode with each alternating as the most negative surface in order to induce photoemission to or from the gyroscope surface. Three different UV sources were used at the other end of the optical fiber: a deuterium arc lamp continuum source[17] and two different Hg discharge line sources (253.7 nm) with different power consumption and drive circuits.[18,19] The results are given in Table II.

Due to unknown geometric factors and transmission co-

TABLE I. Upper bound on quantum efficiency for various materials prepared in gyroscope handling conditions.

Sample material	Measured current (nA)	Upper bound of quantum efficiency
Nb thin film	6.03	9.5×10^{-6}
Nb disk	6.23	9.8×10^{-6}
NbN thin film	11.99	1.9×10^{-5}
Ti disk	9.74	1.5×10^{-5}
Al disk	2.02	3.2×10^{-6}
Mg disk	9.48	1.5×10^{-5}

TABLE II. Photoemission currents and equivalent gyroscope discharge rates with test set-up.

Lamp type	Power usage (W)	Emission from gyroscope (pA)	Equivalent discharge rate (V/h)	Emission to gyroscope (pA)	Equivalent discharge rate (V/h)
D_2 arc[a]	30.0	2.16	16.20	0.09	−0.68
ac Hg discharge[b]	4.4	0.17	1.28	0.02	−0.15
dc Hg discharge[c]	2.8	0.03	0.23	NA	NA

[a]Reference 17.
[b]Reference 16
[c]Reference 18.

efficients, it is difficult to calculate or to measure the total UV flux delivered to the gyroscope's surface in these various configurations, and it is even more difficult to calculate the flux reflected onto the charge control electrode. However, calculations indicate that the quantum efficiency implied by the measurements of electron emission from the gyroscope is consistent with the quantum efficiency measurements of Table I. For example, the 4.4 W Hg discharge lamp is the same lamp used in the quantum efficiency measurements, where it was calculated to have an output of 4.6 mW/cm^2 at a distance of 1.3 cm. This corresponds to a radiance of 7.7 mW/sr, and the lamp's bore diameter is approximately 6 mm. The optical fiber's core has an acceptance solid angle of 0.13 sr and a diameter of 300 μm, and the manufacturer's literature suggests a transmission coefficient of about 0.5 for the 3 m length of fiber used in the experiment. This results in an estimated power at the end of the fiber at 253.7 nm of 1.3 μW, and an upper bound on the quantum efficiency of 1.5×10^{-6}.

On the other hand, it is not known why the electron emission to the gyroscope is so much lower than expected. For example, pure niobium should reflect about 47% of the 253.7 nm photons at normal incidence and ray tracing indicates that only about 14% of this flux should be lost back into the fiber. One strong possibility is that contaminants and oxides on the surface of the niobium coating may be drastically reducing its reflection coefficient. This phenomenon is currently under investigation.

Finally, we proved the charge control concept by controlling the static charge on a levitated, spinning gyroscope with very low charging using the D_2 lamp and a flight prototype fiber-optic fixture. Spurious charging in this system was negligible. The experimental sequence for demonstrating charge control contained the following steps: (a) activate the UV source, (b) set the bias on the charge control electrode to 18 V, (c) allow the system to come to equilibrium, (d) change the bias to -18 V, and (e) set the bias to 0 V. Results in the form of gyroscope potential, measured using the force modulation technique described later, versus time are shown in Fig. 11. Through all of these phases, the static charge on the gyroscope followed the bias on the charge control electrode. The slope of the discharge curve during the transition from $+18$ to -18 V indicates a photocurrent of about 0.2 pA, which is consistent with our direct current measurements on an unlevitated gyroscope as described above.

In conclusion, any of these lamps would provide adequate discharge capability for the science mission given the very small expected charging rates described in the previous section. A mercury discharge lamp with very high radiance is currently being designed by Resonance LTD[19] for use in ground testing and in the upcoming room temperature test flight aboard the Space Shuttle.

The main potential drawback of the photoemission method of discharging the gyroscope is the possible heating of the gyroscope by the UV flux. Under the high vacuum conditions of the GP-B experiment, 10^{-11} mbar, the only cooling mechanism for the gyroscope is provided by thermal radiation. The low thermal emissivity of the gyroscope coating limits the maximum power input to about 3 nW, in order to maintain the gyroscope temperature below 4 K. Calculations show that the heating from the UV flux is smaller than or equal to the heating due to the proton flux for which the system is designed to compensate. Appropriate filtering of all the visible and infrared optical energy from the UV source is necessary. The average energy deposited in the gyroscope per proton is about 50 MeV. Using the data for the worst-case current direction (electron emission to the gyroscope) and the worst-case hypothesis that the gyroscope absorbs all of the UV photon energy, the gyroscope must absorb 1.3×10^7 photons to neutralize each proton. Since each photon has an energy of 4.9 eV, this implies that 64 MeV of UV energy will be deposited for each 50 MeV proton. This is equivalent to about 1 nW for the worst case in which all photons deposit their energy in the gyroscope. In other words, the UV photoemission charge control system will, at worst, compound the gyroscope heating problem by a factor of 2, to about 2 nW; an acceptable level. An alternative approach to charge control, using field emission cathodes, is presently under investigation.[14]

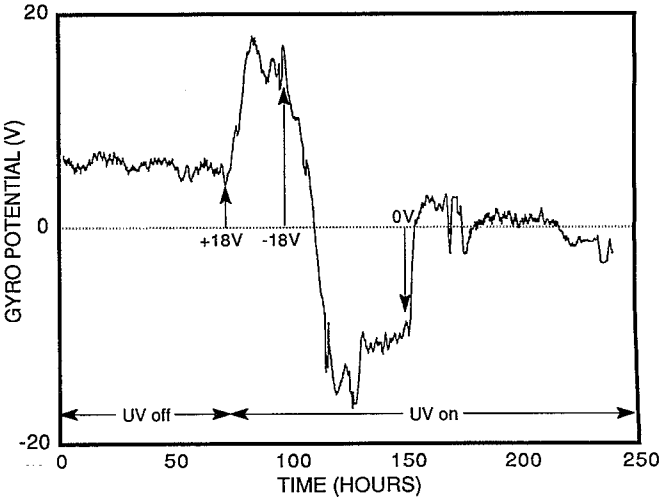

FIG. 11. Charge control of an operational gyroscope with a 254 nm UV fiber-optic system and biases of +18, −18, and 0 V.

IV. $\omega/2\omega$ CHARGE MEASUREMENT METHOD

We start the discussion of charge measurement methods with the $\omega/2\omega$ technique, as this is the most convenient way to develop the needed formalism. This technique is unsuitable for measurements in space, and only useful for ground testing. The GP-B gyroscope utilizes a three orthogonal axes, six electrodes, ac ($\omega/2\pi$=2 kHz) electrostatic suspension technique for the 1 g experiments. The constraint on the suspension system is that the total current into the gyroscope be zero, making it a virtual potential ground

$$\sum_{i=1}^{6} V_{Ei}C_{Ei}=0, \tag{5}$$

where V_{Ei} and C_{Ei} are the voltages and the capacitances of the six electrodes. The force F exerted by one electrode (a spherical cap capacitor) on the gyroscope is given by

$$F=\pi R^2\epsilon_0\frac{V^2}{d_0^2}\left[\frac{1-\cos\theta}{\delta(1-\delta)(1-\delta\cos\theta)}-\frac{1}{\delta^2}\ln\left(\frac{1-\delta\cos\theta}{1-\delta}\right)\right]$$
$$\approx\pi R^2\epsilon_0\frac{V^2}{d_0^2}(1-\cos\theta)\left(\frac{1+\cos\theta}{2}+\frac{2}{3}(1+\cos\theta+\cos^2\theta)\delta\right), \quad (6)$$

where $R=1.9$ cm is the radius of the gyroscope housing, $\theta=28.7°$ and V are the half angle and the voltage of the electrode, $d_0=32$ μm is the gap between the centered gyroscope surface and the electrode, and ϵ_0 is the vacuum dielectric constant. The second part of Eq. (6) is the linearized form in the parameter δ, the fractional displacement of the gyroscope from the center with respect to the gap d_0. This approximation, valid for $\delta\ll 1$, will be used in the following derivation.

As shown in Eq. (5), a centered gyroscope with no charge has zero potential. However we are interested in the case in which a net charge has been transferred to the gyroscope. For this case the total force F_T applied along each of the axes is

$$F_T=B\left(\frac{1+\cos\theta}{2}+\frac{2}{3}(1+\cos\theta+\cos^2\theta)\delta\right)\times(V_1\sin\omega t-V_R)^2$$
$$-B\left(\frac{1+\cos\theta}{2}-\frac{2}{3}(1+\cos\theta+\cos^2\theta)\delta\right)\times(V_2\sin\omega t-V_R)^2 \quad (7)$$

with

$$B\equiv\pi R^2\epsilon_0\frac{1-\cos\theta}{d_0^2},$$

where $V_1\sin\omega t$ and $V_2\sin\omega t$ are the voltages applied to the electrodes, and V_R is the gyroscope potential. In the $1g$ environment V_1 and V_2 are of the order of 1000 and 150 V, respectively. The dc, $\omega/2\pi=2$ kHz, and $2\omega/2\pi=4$ kHz, components of F_T are

$$F_{\rm dc}=B\left((1+\cos\theta)\frac{V_1^2-V_2^2}{4}+\delta(1+\cos\theta+\cos^2\theta)\frac{V_1^2+V_2^2+4V_R^2}{3}\right)=mg', \quad (8)$$

$$F_\omega=2BV_R\left((1+\cos\theta)\frac{V_2-V_1}{2}-\frac{2}{3}\delta(1+\cos\theta+\cos^2\theta)(V_1+V_2)\right)=m\omega^2V_\omega C_\omega, \quad (9)$$

$$F_{2\omega}=B\frac{(1+\cos\theta)\frac{V_2^2-V_1^2}{2}-\frac{2}{3}\delta(1+\cos\theta+\cos^2\theta)(V_1^2+V_2^2)}{2}=4m\omega^2V_{2\omega}C_{2\omega}, \quad (10)$$

where $m=0.063$ kg is the mass of the gyroscope, g' is the projection of the gravitational acceleration along the axis of the two electrodes ($g/\sqrt{3}\leq g'\leq g/\sqrt{2}$), V_ω and $V_{2\omega}$ are the position error voltages at ω and 2ω, and C_ω and $C_{2\omega}$ are the error signal calibration constants at 2 and 4 kHz. For this suspension system the calibration constants are equal, $C_\omega=C_{2\omega}$. Consequently, Eqs. (8)–(10) result in

$$V_R=\frac{V_\omega}{16V_{2\omega}}\left((V_1+V_2)-\frac{8}{3}\frac{V_1V_2\delta(1+\cos\theta+\cos^2\theta)}{(V_1-V_2)(1+\cos\theta)}\right), \quad (11)$$

$$\delta=\frac{3}{1+\cos\theta+\cos^2\theta}\frac{\frac{mg'}{B}-(1+\cos\theta)\frac{V_1^2-V_2^2}{4}}{V_1^2+V_2^2+\left(\frac{V_\omega}{V_{2\omega}}\right)^2\frac{(V_1+V_2)^2}{64}}, \quad (12)$$

where terms of order δ^2 and higher have been ignored.

It is therefore possible to compute both the gyroscope potential and the gyroscope position from easily available parameters, requiring no modifications to the suspension system or to the gyroscope itself. Additionally, the gyroscope position determination can be checked against the position obtained from the suspension capacitance bridge data. The accuracy of this method is only about 30 V, limited by 2 and 4 kHz signal pickup and the nonlinearity in the suspension system. Due to its simplicity this is the method of choice for ground-based testing when a 30 V accuracy is suitable.

This method's applicability to space experiments is limited by the fact that for a centered gyroscope both V_ω and $V_{2\omega}$ are proportional to V_1-V_2, or equivalently to the local acceleration. For GP-B the reduction in acceleration from the ground case by eight orders of magnitude results in $V_1\cong V_2$, and consequently makes this method unusable in space.

V. FORCE MODULATION CHARGE MEASUREMENT METHOD

This is the principal GP-B charge measurement method and is implemented by applying 180° out-of-phase excitation

voltages $V_C \sin(\omega_C t)$ to two opposite electrodes. The frequency ω_C is below the bandwidth of the suspension servo system, while the excitation voltage V_C is much smaller than the suspension voltages V_1 and V_2. In practice we use $\omega_C=5$ Hz and $V_C=5$ V. Taking into consideration this excitation, Eq. (7) is modified to

$$F_T'=B\left(\frac{1+\cos\theta}{2}+\frac{2}{3}(1+\cos\theta+\cos^2\theta)\delta\right)\times(V_1\sin\omega t-V_R-V_C\sin\omega_C t)^2-B\left(\frac{1+\cos\theta}{2}-\frac{2}{3}(1+\cos\theta+\cos^2\theta)\delta\right)\times(V_2\sin\omega t-V_R+V_C\sin\omega_C t)^2. \quad (7a)$$

Using the linear approximation in δ, the components of F_T' at dc, ω_C, and $2\omega_C$ are

$$F_{\omega C}=2BV_RV_C(1+\cos\theta), \quad (13)$$

$$F_{2\omega C}=\tfrac{2}{3}BV_C^2(1+\cos\theta+\cos^2\theta)\delta, \quad (14)$$

$$F'_{\mathrm{dc}}=F_{\mathrm{dc}}+\tfrac{2}{3}BV_C^2(1+\cos\theta+\cos^2\theta)\delta. \quad (15)$$

Equations (13) and (14) reflect the advantages of this method.

(a) With the excitation voltage being applied below its bandwidth, the servo system compensates for the external force applied. Thus, there is no motion of the gyroscope and the total electrostatic force does not change. Notice also that the gyroscope potential and position are fully decoupled in Eqs. (13) and (14).

(b) The gyroscope potential is directly proportional to the control effort signal at ω_C. The proportionality constant is easily determined from the suspension system parameters.

(c) The sign of the control effort signal at ω_C determines the polarity of the gyroscope potential.

(d) The gyroscope potential measurement is independent of the gyroscope position to first order.

(e) The gyroscope displacement from the electric center is directly proportional to the control effort signal at $2\omega_C$. This signal will be used to control the centering of the gyroscope.

(f) The gyroscope position measurement is independent of the gyroscope potential to first order.

(g) This method places no constraints on the bandwidth and the carrier frequency of the servo system.

In practice the gyroscope potential is determined using Eqs. (8), (13), and (15), in the limit $\delta \ll 1$

$$V_R=\frac{F_{\omega C}}{F_{\mathrm{dc}}}\frac{V_1^2-V_2^2}{8V_C}, \quad (16)$$

where the ratio $F_{\omega C}/F_{\mathrm{dc}}$ is equal to the ratio of the feedback control effort signals at ω_C and dc. The sensitivity of this charge measurement method is limited by the noise in the control effort signal near the frequency at which the excitation voltage is applied to the electrodes. The measured control effort noise is $10^{-5}\ g/\sqrt{\mathrm{Hz}}$. In space, the control effort noise is expected to be smaller than $10^{-9}\ g/\sqrt{\mathrm{Hz}}$. If the excitation voltage is also reduced to $V_C=25$ mV, then the estimated sensitivity of the charge measurement system is $\Delta V_R=0.04\ \mathrm{V}/\sqrt{\mathrm{Hz}}$ or $\Delta V_R=4$ mV in 100 s. Considering the requirement that $V_R \leqslant 15$ mV, this represents a very good gyroscope charge measurement performance, making force modulation the method of choice for both space and ground-based experiments. The force modulation charge measurement produces a gyroscope disturbing torque which scales as $V_C^2/V_{1,2}^2$ with respect to the dominant electrostatic support disturbing torque. As $V_{1,2}\approx 0.3$ V, the gyroscope drift due to V_C will be less than 1% of the 10^{-11} deg/h drift caused by the electrostatic support.

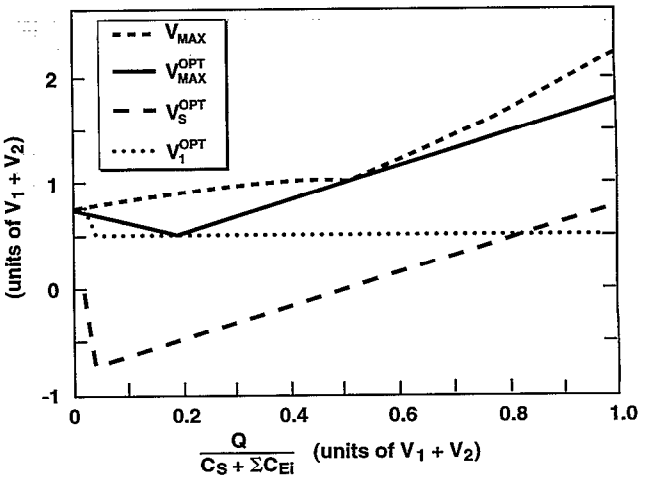

FIG. 12. dc supplementary electrode calculation. Plotted as a function of $V_R'\equiv Q/(C_S+\Sigma C_{Ei})$ are: (1) the maximum electric field with zero supplementary support $V_{\max}$, (2) the minimized maximum electric field using supplementary support $V_{\max}^{\mathrm{opt}}$, (3) the supplementary support voltage required for the minimization V_S^{opt}, (4) the ac electrode voltage at the optimal conditions V_1^{opt}.

VI. dc SUPPLEMENTARY SUPPORT CHARGE MEASUREMENT METHOD

The electric fields necessary for ground-based levitation of the GP-B gyroscope are near the level where electron field emission and consequently charging occur. The peak electric field can be significantly reduced by using the coating covering the upper hemisphere of the gyroscope housing (not occupied by the ac suspension electrodes) for additional electrostatic support. For ground testing purposes we operate this supplementary electrode in a dc mode.

Figure 12 shows the results of a calculation of the electric fields in the gyroscope as a function of the gyroscope potential. Plotted as a function of gyroscope charge are: (1) the maximum electric field with no supplementary support, (2) the optimally reduced maximum electric field using supplementary support, (3) the supplementary support voltage required for this optimization, (4) the ac electrode voltage at the optimal condition. A significant reduction of the maximum electric stress occurs for gyroscope charging levels around $V_R=0.2(V_1+V_2)$. Zero control effort, $V_1=V_2$, is required for the optimal reduction in the field stress of a centered gyroscope. In these conditions the dc excitation

voltage V_S applied to the supplementary electrode gives a direct measure of the gyroscope charge. The electric potential V_R for a centered gyroscope is given by

$$V_R=\left(Q+V_SC_S+\sum_{i=1}^{6}\mathbf{V}_{Ei}C_{Ei}\right)\Big/\left(C_S+\sum_{i=1}^{6}C_{Ei}\right)$$

$$=(Q+V_SC_S)\Big/\left(C_S+\sum_{i=1}^{6}C_{Ei}\right), \quad (17)$$

where Q is the charge of the gyroscope, C_S is the capacitance of the gyroscope to the supplementary electrode, and the second equality uses Eq. (5). The force F_S applied by the dc supplementary electrode to the gyroscope is

$$F_S=B'(V_S-V_R)^2$$

$$=B'\left(\frac{V_S\Sigma C_{Ei}-Q}{C_S+\Sigma C_{Ei}}\right)^2=mg, \quad (18)$$

where B' is the geometric factor describing the supplementary electrode and mg is the weight of the gyroscope. For a gyroscope with $Q=0$, requiring a dc excitation voltage V_{S0}, Eq. (18) becomes

$$B'\left(\frac{V_{S0}\Sigma C_{Ei}}{C_S+\Sigma C_{Ei}}\right)^2=mg. \quad (18a)$$

From Eqs. (18) and (18a) the gyroscope charge Q is given by

$$Q=(V_S-V_{S0})\sum_{i=1}^{6}C_{Ei}. \quad (19)$$

The dc excitation voltage V_{S0} required for the levitation of an uncharged gyroscope with $V_1=V_2$ (zero control effort of the ac suspension) is easily measured and/or calculated. Therefore the dc excitation voltage V_S required for the levitation of a charged gyroscope at zero control effort of the ac suspension is a direct measure of the gyroscope charge Q. This result can be generalized for the case of a nonzero ac control effort, and for the case of a noncentered gyroscope. The sensitivity of this method is about 5 V. Its main disadvantage is that it requires supplementary electrodes.

In conclusion, we have demonstrated that the UV charge control technique coupled with the force modulation charge measurement method will satisfactorily solve the charging problem for the cryogenic GP-B gyroscopes in both space mission and ground testing environments. These same techniques are also generally applicable to levitating systems requiring bipolar charge control performed with a minimum of disturbance.

ACKNOWLEDGMENTS

We would like to thank Richard Van Patten for useful discussions, Joseph Fiero for the calculation of the yield of secondary electrons, and Monica Jarnot for editorial assistance. This work was supported by NASA Contract No. NAS8-36125.

[1] J. P. Turneaure, C. W. F. Everitt, and B. W. Parkinson, Adv. Space Res. **9**, 29 (1989).
[2] L. I. Schiff, Proc. Natl. Acad. Sci. **46**, 871 (1960).
[3] Staff of Space Department, Johns Hopkins University and Staff of Guidance and Control Laboratory, Stanford University, J. Spacecraft **11**, 637 (1974).
[4] G. M. Keiser, S. Buchman, J. V. Breakwell, S. Feteih, D. Gill, J. P. Turneaure, and Y. M. Xiao, Proceedings of 12th International Conference on General Relativity and Gravitation, Boulder, Colorado, 1989 (unpublished).
[5] F. London, *Superfluids* (Dover, New York, 1961), Vol. I.
[6] R. V. Latham, *High Vacuum Voltage Insulation: The Physical Basis* (Academic, London, 1981).
[7] P. Zhou, S. Buchman, K. Davis, C. Gray, and J. P. Turneaure, Surf. Coat. Technol. **54/55**, 548 (1992).
[8] J. I. Vette, *The NASA/National Space Science Data Center Trapped Radiation Environment Model Program (1964–1991)*, NSSDC/WDC-A-R&S 91-29 (1991).
[9] J. Feynman, G. Spitale, J. Wang, and S. Gabriel, J. Geophys. Res. **98**, 13281 (1993).
[10] H. A. Enge, *Introduction to Nuclear Physics* (Addison-Wesley, Reading, MA, 1966).
[11] P. Couisinie, N. Fert Columbie, and R. Simon, Compte Rendu **249**, 387 (1959).
[12] Y. Boudon, These de doctorat d'Etat, Universite Pierre et Marie Curie, 1984.
[13] W. L. Imhof and J. B. Reagan, J. Geophys. Res. Space Phys. **74**, 5054 (1969).
[14] S. Buchman, T. Quinn, G. M. Keiser, and D. Gill, J. Vac. Sci. Technol. B **11**, 407 (1993).
[15] *Landolt-Bornstein* (Springer, Berlin, 1959), Vol. II, Part 6, p. 991.
[16] Model No. 78-2046-1, Jelight Corporation, 23052 Alcade #E, P. O. Box 2632, Laguna Hills, CA 92654.
[17] Model No. 63163 with 60055, Oriel Corporation, 250 Long Beach Blvd., P. O. Box 872, Stratford, CT 06497.
[18] G. P. Adams, G. K. Rochester, T. J. Sumner, and O. R. Williams, J. Phys. E: Sci. Instrum. **20**, 1261 (1987).
[19] Resonance Ltd., 171 Dufferin St. S. Alliston, Ontario LOM 1A0, Canada.